Fluid Flow Induced by Seismic Waves in Fractures

Youcef Bouzidi[1], Nabil Kharoua[2], Fateh Bouchaala[1], Hamid Ait Abderahmane[3], and Douglas, R. Schmitt[4]

[1]Department of Earth Sciences, Khalifa University of Science and Technology, Abu Dhabi, PO. Box 127788 UAE
[2]Department of Mechanical Engineering, Ecole Nationale Polytechnique de Constantine, BP 75, A, Nouvelle Ville RP, Constantine, Algeria
[3]Department of Mechanical Engineering, Khalifa University of Science and Technology, Abu Dhabi, PO. Box 127788 UAE
[4]Department of Earth, Atmospheric, and Planetary Sciences, Purdue University, 550 Stadium Mall Drive, West Lafayette, IN 47907-2051, U.S.A

Corresponding author: Fateh Bouchaala (fateh.bouchaala@ku.ac.ae).

ABSTRACT

A theoretical and numerical analysis is presented on the squeezed film of an incompressible fluid between two parallel fracture walls induced by seismic waves at normal incidence. In the frame of small oscillations, a closed form of the fluid pressure changes along with the fracture, and the fluid velocity field distribution is proposed. The developed analytical solutions are valid for any relative amplitude and phase of the vibrations within the assumed small oscillations and can help in understanding the induced fluid flow in fractures near zero-offset seismic wave propagation in a fluid-saturated fractured reservoir with nearly parallel fracture walls. It is found that the fluid flow is governed by the squeezing motion due solely to the difference of the vertical fluid velocities. In the absence of experimental data, the analytical solutions are validated with numerical solutions of the full Navier-Stokes equations. The comparison confirms the accuracy of the analytical solutions, showing that average fracture pressure rises with frequency, fracture length squared, and decreasing wall separation. It is also found that the presence of a pressure gradient does not hinder the overall flow during an oscillation cycle. The high induced horizontal acceleration of the fluid can reduce surface tension and improve oil to dissolve in any injected solvents. This may help mobilize fluids in fractured reservoirs, potentially explaining the improved oil recovery observed with surface seismic wave stimulation near production wells. Optimizing flow parameters through accurate fracture characterization can further enhance oil recovery.

Keywords

Fractures, Improved Oil Recovery, Navier-Stokes equations, Seismic Induced Fluid Flow, Seismic Waves.

I. INTRODUCTION

The Improved Oil Recovery (IOR) of hydrocarbons via seismic wave stimulation has been discussed since the 1950's but is still not extensively covered in the literature. Comprehensive reviews of this topic are given by (1), Irfan, Lenn (2), and Sun, Retnanto (3). Positive results have been reported regarding enhanced oil production through reservoir stimulation by seismic waves at the surface near an oil production well. Seismic wave stimulation can play an important role in enhanced oil recovery and can be achieved using a single tool at a lower cost and with minimal environmental impact (4). Pride, Flekkøy (5) reported that seismic stimulation affects fluids at the pore-scale level by sending waves across a reservoir to mobilize patches of oil leading to an increase in production level. They modeled this effect numerically and gave an analytical expression for a well-defined seismic amplitude above which the perturbation created by the waves can mobilize trapped oil. Allahverdiyev (6) showed a potential production mechanism improving sweep efficiency and estimating increased production. The improvement is due to fluid pressure oscillations as explained by a viscous crossflow between different permeable layers. Kouznetsov, Simkin (7) reported results of laboratory experiments and tests on natural core samples extracted from Russian oilfields and on synthetic sand packs. They noticed that the displacement of oil is due to an increase of water in the presence of vibro-energy. Seismic stimulation is also used in boreholes. Westermark, Brett (8) presented a promising field pilot test to demonstrate the potential of downhole vibration stimulation in a water flooded shallow reservoir in Osage County, Oklahoma. In this contribution we adapted the mechanical engineering 'squeeze-flow' problem of oscillating two fracture walls that was developed to understand problems in lubrication to seismic vibrations near normal incidence. As such, the analytical solutions given thereafter are not developed to study quantitative reflectivity and transmissivity of seismic waves through fractures, but rather to explain one possible mechanism that could lead to improved oil recovery under certain conditions.

Improved oil recovery is not yet a mature subject. Despite numerous secondary oil recovery methods, modern recovery rates still do not exceed 50%, making research to improve oil recovery highly welcomed by the industry. IOR and EOR (improved/enhanced oil recovery) methods are directly related to fluid flow and its distribution in the reservoir. Both characteristics are controlled by fracture networks in the reservoir. Therefore, obtaining comprehensive information about fractures is crucial for IOR and EOR studies. Fractures' orientations, locations, densities, apertures and infilling materials are the most desired information for IOR and EOR studies. Fractures are more compliant than the rock matrix. Consequently, the mechanical response of a fractured medium can be dominated by the mechanical behavior of the fractures within it (9). The weak stiffness (high compliance) of fractures causes a reduction and azimuthal dependence in seismic amplitude and velocity

of seismic waves travelling within a fractured medium(e.g. 10, 11). The presence of fractures also leads to a frequency dependence of rock stiffness, which is commonly known as the dispersion phenomenon (12). Pyrak-Nolte, Myer (13) attributed the frequency dependence of fracture stiffness to a simple consequence of the subset of apertures sampled by a given frequency. Therefore, a multi-scale frequency study of seismic wave propagation can enhance our knowledge of fracture systems on a scale ranging from microns to the order of meters. However, the success of these studies requires a good signal to noise ratio (S/N) of seismic data. Such data sets can be provided by three component (3C) zero offset vertical seismic profiling (3C-ZVSP, 5-130 Hz) or full waveform sonic logs (in the order of kHz) data.

Fluid dynamics and properties play an important role (14) in addition to fracture lengths and apertures. To further understand fluid flow in fractures we present a possible mechanism that can contribute to improved oil recovery. This will be derived through Navier-Stokes equations by adapting the squeeze fluid flow problem, well-known in mechanical engineering applications, to seismic vibrations. In this development, the fractures are assumed to be horizontal with parallel walls (Fig. 1). The squeeze flow problem involves the study of induced pressures and the resulting fluid flows between two parallel plates moving relative to each other in the direction normal to the plates (Fig. 1). This problem has been the subject of interest of several studies and is relevant in a wide range of industrial applications that include aerospace, naval, medical, and nuclear(see e.g., 15, 16-21). The squeeze flow effects have been studied thoroughly under various conditions and assumptions and are traditionally relevant to lubrication applications as well as to subdue instability and vibration issues(see e.g., 15, 17, 18, 21, 22). These effects have been studied in dynamic Micro Electro-Mechanical Systems (MEMS) devices (see e.g., 23, 24, 25) and in medical applications(see e.g., 16, 19, 20, 26). (27) has studied radial fluid flow between two parallel plates to estimate inertial effects. He assumed that the flow is purely radial, i.e., the fluid flow velocities are identically zero in both the parallel z and azimuthal θ directions of the plates. In this case, the flow is governed solely by the Navier-Stokes equations in the radial direction and by the continuity equation. Under the assumption of fluid incompressibility, the continuity equation enables the Navier-Stokes equations to be simplified (see (4) in Livesey (27)). He gave an approximate solution as a parabolic velocity distribution that satisfies the continuity equation and has shown that the inertia effects are large enough to change the sign of the radial fluid pressure gradient at low Reynolds numbers.

Later, Thorpe (28) has derived an ordinary differential equation (ODE) from the Navier-Stokes and the continuity equations. He argued that a two-parameter similarity solution always exists for fluid velocity because the ODE could be derived. The resulting ODE is non-linear and has no known general solution but can be solved numerically. However, Gupta and Gupta (29)

have shown that not all velocity profiles lead to a similarity solution and argued that Thorpe (28) failed to recognize that the transverse Reynolds number R is time dependent in the derived ODE (see (13) in Thorpe (28)) and gave a counter example for constant plate velocity, for which no similarity solution exists. In his theoretical development, Thorpe (28)solved the ODE for fluid velocity in the case of constant plate velocity using a perturbation approach that led to a solution valid for small Reynolds numbers and for plates moving either away from or towards each other with the same velocity and amplitude. He further presented a theoretical and experimental investigation of air loads effects on a rigid plate oscillating in the direction normal to a fixed surface. The approach considers air compressibility under the presumption that it is an ideal gas. The pressure solution to the problem was given for a narrow gap between the plates, filled with an ideal gas, compared to its other dimensions, by neglecting the normal velocity of the fluid. These assumptions have allowed a significant simplification of the Navier-Stokes and continuity equations. This approach led to a solution as a power series for the pressure distribution in the fluid.

Several other approximations modeling the dynamic behavior of fluids between parallel plates of various shapes and structures can be found in the literature(23, 24, 30). Under the same assumptions as those used by Livesey (27), Jackson (31) presented an iterative scheme to find both the horizontal pressure gradient and velocity to the squeeze flow problem for an unsteady motion of a rigid disc relative to a fixed plane. He compared the relative inertial and viscous effects. Starting with a uniform velocity profile and the overall continuity integral, he has estimated both horizontal fluid pressure gradient and velocity and has shown that the process is rapidly converging after two iterations. The literature on the squeeze flow problem is dominated either by solving the case of i) one disc/plate moving with respect to a fixed plane or ii) two discs/plates moving, either away from or towards each other, with velocities of the same magnitudes. Consequently, all these squeeze flow models cannot describe seismic wave vibrations of the fracture walls which do not necessarily always move towards or away from each other with the same amplitude and phase.

In this contribution, the squeeze-flow problem is modified and adapted to seismic vibrations. To achieve this goal the plates must mimic the two walls of a fracture but, these are now allowed to vibrate independently with no restrictions on their respective relative amplitudes and phases. However, the displacements accompanying seismic waves are small and the walls do not make contact at any time. This assumption allows the Navier-Stokes equations to be linearized by dropping the convection terms. This will be compared later through numerical simulations that include all terms of the Navier-Stokes equations due to the lack of relevant experimental data. The problem is solved separately for each plate for the velocity and pressure profiles and then the overall solution is obtained using the principle of superposition, a well-known and accepted

principle in seismic wave propagation assuming the flow is laminar. This can be a step further in understanding the mechanisms in reservoir production stimulation through seismic vibrations at the surface near an oil well. This may also provide insight into the transient pressure disturbances that might be encountered on faults contributing to the dynamic triggering of seismicity, which have largely ignored the role of induced fluid pressure (32, 33).

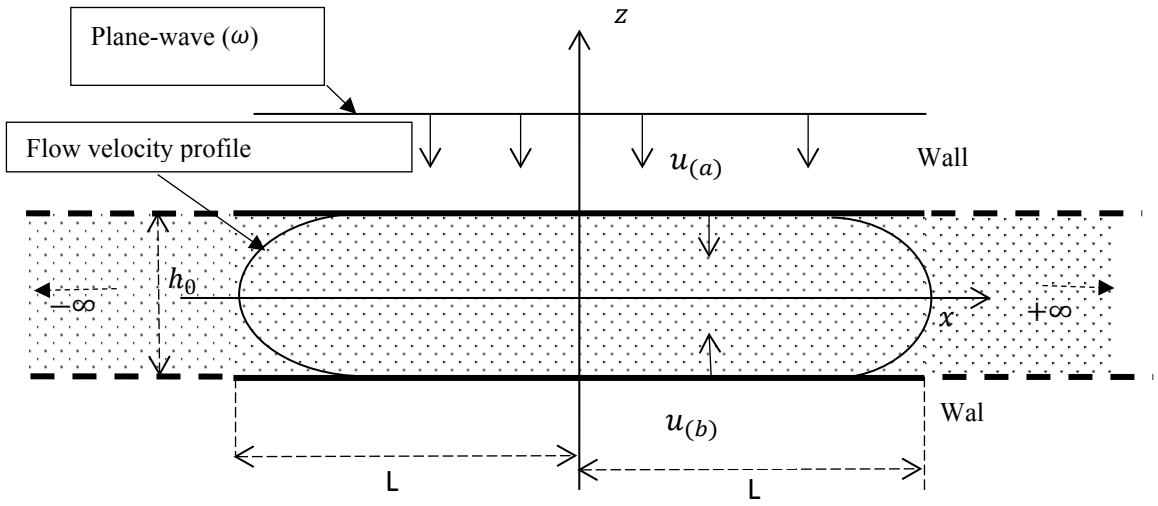

Figure 1. Reference frame and thin fluid film between two rigid and vertically vibrating parallel fracture walls. The walls are assumed to extend laterally to infinity on both sides. The parabolic velocity profile is shown for a compressional phase.

II. METHODOLOGY

A suitable complex formulation will be employed to derive analytical solutions in the complex plane. The real parts are the actual physical solutions of the problem. Consider two-dimensional fluid flow between two parallel fracture walls (a) and (b) as shown in Fig. 1. The two walls have a length of 2L and are separated by a distance h_0 which is much smaller than $2L$ ($h_0 \ll L$) to neglect the edge effects. Let μ and ρ denote the dynamic viscosity and density of a saturating incompressible fluid, respectively.

To find the solution when both fracture walls oscillate with amplitudes and phases that are not necessarily equal or opposite to each other, we solve the problem by finding solutions for the case when only one wall oscillates. Here, we adopt a complex form for the displacements u_a and u_b and let the upper and bottom walls (a) and (b) oscillate vertically with amplitudes ε_a and ε_b and phases φ_a and φ_b, according to

$$u_a = \varepsilon_a e^{i(\omega t+\varphi_a)} \quad (1)$$

and

$$u_b = \varepsilon_b e^{i(\omega t+\varphi_b)} \quad (2)$$

respectively. The vertical velocities of the walls are the time derivatives of (1) and (2). It is worth mentioning that the physical displacements are given by the real parts of u_a and u_b.

To solve the problem, the principle of superposition for small oscillations is used. As such, the problem when the bottom wall is assumed at rest and when the upper wall is at rest will be solved separately. The two solutions are then combined through the superposition principle to achieve the solution of both walls oscillating without any restrictions on the phases and amplitudes.

First, assume that the bottom wall is at rest in the reference frame given in Fig. 1, at any time t, the distance between the two walls is

$$h(t) = h_0 + \left(\frac{u_a + u_a^*}{2}\right) \tag{3}$$

where the symbol * denotes the complex conjugate. Following Thorpe (28), Gupta and Gupta (29) but using complex valued quantities, let $\xi = \frac{2z}{h}$ be a dimensionless space variable where the time dependence is dropped for clarity and let the kinematic viscosity be $\eta = \mu/\rho$. Replacing z with ξ, the Navier-Stokes and continuity equations for two-dimensional flow in the absence of body forces are

$$\frac{\partial v_x}{\partial t} + v_x\frac{\partial v_x}{\partial x} + v_\xi\frac{2\partial v_x}{h\,\partial \xi} = -\frac{1}{\rho}\frac{\partial p}{\partial x} + \eta\left(\frac{\partial^2 v_x}{\partial x^2} + \frac{4}{h^2}\frac{\partial^2 v_x}{\partial \xi^2}\right) \tag{4}$$

$$\frac{\partial v_\xi}{\partial t} + v_\xi\frac{2\partial v_\xi}{h\,\partial \xi} + v_x\frac{\partial v_\xi}{\partial x} = -\frac{1}{\rho}\frac{2}{h}\frac{\partial p}{\partial \xi} + \eta\left(\frac{\partial^2 v_\xi}{\partial x^2} + \frac{4}{h^2}\frac{\partial^2 v_\xi}{\partial \xi^2}\right) \tag{5}$$

$$\frac{\partial v_x}{\partial x} + \frac{2\partial v_\xi}{h\,\partial \xi} = 0 \tag{6}$$

Another interesting case is when a constant pressure gradient exists between the inlet and outlet of a fracture of length 2L with a pressure difference of $p_{-L} - p_L > 0$. Assume a steady Newtonian viscous fluid flow in a fracture with parallel walls, a narrow gap of depth h_0, and a large width. Neglecting the edge effects at the inlet and the outlet, i.e. the flow is fully developed, only one non-zero velocity component exists in the x direction (no variation of the velocity in the y direction perpendicular to the upward z-direction. Neglecting gravity effects, the velocity profile, given in details in Wikes(34), can be adapted to the reference frame used here. The pressure is represented by a linear function $p_0 = a + bx$, where a and b can be found by the inlet and exit conditions.

$$p = -\frac{p_{-L} - p_L}{2L}x + \frac{p_L + p_{-L}}{2} \tag{7}$$

Using Wikes (34) the fluid velocity, independent of x is given by

$$v_x = \frac{1}{2\eta\rho}\left(\frac{\partial p}{\partial x}\right)z^2 + c_1 z + c_2 \tag{8}$$

where c_1 and c_2 can be found using the boundary conditions at the two walls where the velocity field vanishes, assuming that the vertical gap change is small. We have

$$v_x = -\frac{1}{2\eta\rho}\left(\frac{\partial p}{\partial x}\right)(hz - z^2) \tag{9}$$

Letting $z = \frac{h}{2}\xi$ leads to

$$v_x = -\frac{h_0^2}{8\eta\rho}\left(\frac{\partial p}{\partial x}\right)(2\xi - \xi^2) \tag{10}$$

Assuming a constant pressure gradient $\gamma = \frac{\partial p}{\partial x}$ and seeking solutions for the problem of vibrating fracture walls where the vertical fluid velocity is cast in separated variables form, space and time, by introducing a function $f_a(\xi)$, independent of time, that describes solely the vertical spatial variation at any instant t and is modulated by the velocity $\dot{u}_a$ (see e.g.Thorpe (28);Gupta and Gupta (29)). Explicitly,

$$v_\xi(\xi,t) = f_a(\xi)\dot{u}_a \tag{11}$$

Note that the subscript a refers to the moving upper wall (a).

Using (11) and integrating with respect to x, the continuity (6) leads to

$$v_x(x,\xi,t) = -\frac{2}{h}x f'_a\dot{u}_a + q(\xi,t) \tag{12}$$

Using the velocity at $x = 0$, we obtain $q(\xi,t)$ leading to

$$v_x(x,\xi,t) = -\frac{2}{h}x f'_a\dot{u}_a - \frac{\gamma}{8\eta\rho}h_0^2(2\xi - \xi^2) \tag{13}$$

where f'_a represents the first derivative of $f_a(\xi)$ with respect to ξ. The dot on the displacement refers to the first derivative with respect to time (velocity). For clarity, the variable ξ is dropped from f hereafter.

For small oscillations (acoustic approximation), only first order terms are retained, the convection terms can be dropped, using the fact that the vertical fluid velocity is independent of x, and $h(t)$ approximated by h_0, (4) and (5) are reduced to

$$\frac{\partial v_\xi}{\partial t} = -\frac{1}{\rho}\frac{2}{h_0}\frac{\partial p}{\partial \xi} + \eta\frac{4}{h_0^2}\frac{\partial^2 v_\xi}{\partial \xi^2} \tag{14}$$

$$\frac{\partial v_x}{\partial t} = -\frac{1}{\rho}\frac{\partial p}{\partial x} + \eta\frac{4}{h_0^2}\frac{\partial^2 v_x}{\partial \xi^2} \tag{15}$$

II.1 Boundary Conditions

To solve (14) and (15) we apply the natural boundary conditions of the problem, which are, on one hand, the horizontal fluid

velocity vanishes (i.e., the no slip assumption) at both walls' surfaces. Explicitly we have

$$v_x(x,0,t) = 0, v_x(x,2,t) = 0 \tag{16a}$$

or equivalently

$$f_a(0) = 0 \text{ and } f_a(2) = 1 \tag{16b}$$

On the other hand, the vertical fluid velocity is nil at $\xi = 0$ but equal to that of the moving wall at $\xi = 2$. Explicitly we have

$$v_\xi(x,0,t) = 0, v_\xi(x,2,t) = \dot{u}_a \tag{17a}$$

or equivalently

$$f'_a(0) = 0 \text{ and } f'_a(2) = 0 \tag{17b}$$

Using the proposed solutions (11) and (13) in (14) and (15) and then taking the derivative with respect to x and ξ, respectively, we get

$$\frac{\omega h_0^2}{\eta} f''_a + 4i f''''_a = 0 \tag{18}$$

Here f''_a and f''''_a are the second and fourth derivative of f_a with respect to ξ. The coefficient of the first term of (18) is known as the modified Reynolds number ($R_e = \frac{\omega h_0^2}{\eta}$). Another quantity that is commonly known in the literature as the shear wave number, sometimes referred to as Stokes number, is $s = \sqrt{R_e}$. Using the boundary conditions at $\xi = 0$ and $\xi = 2$, then translating the ξ axis to the middle of the gap (now ξ varies in $[-1, 1]$), the solution to (18) is

$$f_a = c\left[e^{\frac{s}{2}\sqrt{i}(\xi+1)} - e^{-\frac{s}{2}\sqrt{i}(\xi-1)} - \frac{s}{2}\sqrt{i}\left(e^{s\sqrt{i}} + 1\right)\xi\right] + c\left[e^{s\sqrt{i}} - \frac{s}{2}\sqrt{i}\left(e^{s\sqrt{i}} + 1\right) - 1\right] \tag{19}$$

Here, c is given by:

$$c = \frac{1}{2(e^{s\sqrt{i}}-1) - \sqrt{i}s(e^{s\sqrt{i}}+1)} \tag{20}$$

It is important to note that (18) does not depend on the second term of (13). Second, the solution when the upper wall is assumed fixed, using the proper boundary conditions, frame of reference, and translation of the ξ axis, is found as

$$f_b = -c\left[e^{\frac{s}{2}\sqrt{i}(\xi+1)} - e^{-\frac{s}{2}\sqrt{i}(\xi-1)} - \frac{s}{2}\sqrt{i}\left(e^{s\sqrt{i}} + 1\right)\xi\right] + c\left[e^{s\sqrt{i}} - \frac{s}{2}\sqrt{i}\left(e^{s\sqrt{i}} + 1\right) - 1\right] \tag{21}$$

It is readily noticeable that the solution f_b is a mirrored function of f_a around $\xi = 0$ and that both functions have two terms, the first is ξ dependent and the second is ξ independent.

II.2 Fluid Velocities and Pressure

Using the principle of superposition of the two solutions developed for one wall fixed, the general solution for the vertical fluid velocity is

$$v_\xi(\xi,t) = c\left[e^{\frac{s}{2}\sqrt{i}(\xi+1)} - e^{-\frac{s}{2}\sqrt{i}(\xi-1)} - \frac{s}{2}\sqrt{i}\left(e^{s\sqrt{i}}+1\right)\xi\right](\dot{u}_a - \dot{u}_b) + c\left[e^{s\sqrt{i}} - \frac{s}{2}\sqrt{i}\left(e^{s\sqrt{i}}+1\right) - 1\right](\dot{u}_a + \dot{u}_b) \qquad (22)$$

The vertical velocity has two terms. A first term that is ξ dependent and a second term that is ξ independent which are proportional to the difference and the sum of the velocities of the walls, respectively. According to the relative phase of the velocities of the walls, a vertical translation of the fluid can occur when the displacements of the walls are synchronised. First, assume that the amplitudes ε_a and ε_b in (1) and (2) are equal. On one hand, when the phases of the velocities φ_a and φ_b are equal (equivalently $\dot{u}_a = \dot{u}_b$) only a vertical translation of the fluid, independent of ξ, occurs. On the other hand, when the velocities are out of phase by 180^o (equivalently $\dot{u}_a = -\dot{u}_b$) only a compression (or expansion) of the fluid, occurs. In all other combinations of amplitudes and phases of the velocities of the fracture walls, both terms of (22) contribute to the translation and compression (or expansion) of the fluid between the walls. Identically to the vertical velocity, the general solution for the horizontal fluid velocity is obtained by combining the two separate solutions when the upper or the bottom wall is fixed. Moving the ξ axis origin to the center of the gap (ξ varies between -1 and 1) lead to

$$v_x(x,\xi,t) = -x\frac{s}{h_0}c\sqrt{i}\left(e^{\frac{s}{2}\sqrt{i}(\xi+1)} + e^{-\frac{s}{2}\sqrt{i}(\xi-1)} - e^{s\sqrt{i}} - 1\right)(\dot{u}_a - \dot{u}_b)\frac{\gamma h_0^2}{8\eta\rho}\left(1-\xi^2\right) \qquad (23)$$

It is also noticeable that when $\dot{u}_b = \dot{u}_a$ no squeeze occurs. Consequently, no fluid flow is generated by the oscillation in both the vertical and horizontal directions as discussed above. It is worth highlighting that the ansatz or the predefined function given by (11) for the vertical velocity component leads to a horizontal velocity profile that does not follow the Nusselt's parabolic shape, but a profile based on $s = \sqrt{R_e}$ where ($R_e = \frac{\omega h_0^2}{\eta}$). The fluid flow acceleration in the horizontal direction is

$$a_x(x,\xi,t) = -i\sqrt{i}\omega\frac{s}{h_0}c\left(e^{\frac{s}{2}\sqrt{i}(\xi+1)} + e^{-\frac{s}{2}\sqrt{i}(\xi-1)} - e^{s\sqrt{i}} - 1\right)(\dot{u}_a - \dot{u}_b)x \qquad (24)$$

Using the same reasoning, the pressure-variation laterally along the fracture is found as

$$p = -i\frac{2\sqrt{i}}{3}\omega s L^2 c\frac{\rho}{h_0}\left(e^{s\sqrt{i}}+1\right)[x^2 - L^2](\dot{u}_a - \dot{u}_b)\frac{p_{-L}-p_L}{2L}x + \frac{p_{-L}+p_L}{2} \qquad (25)$$

In this case the pressure gradient is time and x dependant and is given by

$$\frac{\partial p}{\partial x} = -i\frac{4\sqrt{i}}{3}\omega s L^2 c\frac{\rho}{h_0}\left(e^{s\sqrt{i}}+1\right)x(\dot{u}_a - \dot{u}_b) - \frac{p_{-L}-p_L}{2L} \qquad (26)$$

As (25) depicts, the pressure distribution laterally in the fracture is independent of the dimensionless variable ξ. The actual physical pressure is the real part of (25). The average pressure laterally along the fracture is found by integrating (25) along the walls' length. Explicitly we have

$$p = -i\frac{2\sqrt{i}}{3}\omega s L^2 c\frac{\rho}{h_0}\left(e^{s\sqrt{i}}+1\right)(\dot{u}_a - \dot{u}_b) + \frac{p_{-L}+p_L}{2} \tag{27}$$

This result can be regarded as the resistance of the fluid to the motion of the walls. The result for the pressure obtained here can be compared to that derived by Thorpe (28) (see his (38)) by taking only the first order terms. Indeed, Thorpe (28) has given an approximate fluid pressure for a sinusoidal wall motion with velocities of same magnitude but out of phase by 180^0. Explicitly he assumed that the vertical variation of pressure (or velocities) is negligible and only (14) subsists and reduces to

$$\frac{\partial v_x}{\partial t} + v_x\frac{\partial v_x}{\partial x} = -\frac{1}{\rho}\frac{\partial p}{\partial x} + \eta\frac{4}{h^2}\frac{\partial^2 v_x}{\partial \xi^2} \tag{28}$$

He obtained the solution numerically following the iterative scheme given by Jackson (31). However, Thorpe did not provide the actual solution for the function $f(\xi)$ but rather gave an approximate solution for the pressure for a sinusoidal wall motion obtained numerically as described byJackson (31). Moreover, the solutions developed by Jackson (31) and that of Thorpe (28) are only valid for walls moving towards or away from each other with velocities of same magnitudes. In contrast, the result developed here is an exact analytical solution of (4), (5), and (6) using a solution of the form given by (11), under the assumption of small oscillations and long wavelength plane waves normally incident onto the upper wall (Fig. 1). Furthermore, in contrast with the solution given by Thorpe (28), the solutions given here are generalized for any relative oscillations of the walls which can differ both in amplitude and phase. For the specific case where the two walls vibrate with the same amplitude but are 180° out phase, for example, the pressure across the fracture given by (24) reduces to

$$p = -i\frac{4\sqrt{i}}{3}\omega s L^2 c\frac{\rho}{h_0}\left(e^{s\sqrt{i}}+1\right)[x^2 - L^2]\dot{u}_a - \frac{p_{-L}-p_L}{2L}x + \frac{p_{-L}+p_L}{2} \tag{29}$$

Again here, this result is simply obtained as a particular case described by (24) by setting $\varphi_b = \varphi_a + \pi$ and $\varepsilon_a = \varepsilon_b$, or equivalently $\dot{u}_a = -\dot{u}_b$.

It is important to note that the fluid flow is characterized by two Reynolds numbers when the second order terms are included (28). One term, $R_1 = \frac{\omega h_0^2}{\eta}$, is linked to the first order inertia term. For example, for a ratio of 0.05, the second order term contributes about 6%. Another term, $R_2 = \frac{\omega h_0 \varepsilon}{\eta}$ where ε is the amplitude of the oscillation which is linked to the second order term. The ratio $\frac{R_2}{R_1} = \frac{\varepsilon}{h_0}$ measures the contribution of the second order term to the overall fluid flow. Therefore, the second order term is small when,

$$\varepsilon \ll h_0 \tag{30}$$

which is the case for seismic vibrations. In other words, R_2 must be much smaller than R_1. However, there is no restriction on the value of R_1but must be within the limit of laminar flow. In the absence of a steady flow due to a pressure gradient only the first term survives in (24)-(26) and (28).

III. Numerical Validation with Computational Fluid Dynamics

Experiments are very difficult to conduct for validation purposes. Instead, the proposed analytical solutions will be compared to numerical solutions obtained using the finite volume technique using the full Navier-Stokes equations to assess their domain of validity. To ensure that the developed analytical solutions are accurate, the calculated pressure drop across the fracture and velocity fields were compared to a full numerical solution of the Navier-Stokes equations (4), (5), and (6) using Computational Fluid Dynamics (CFD) scheme. The numerical results are then compared to the theoretical field variables of velocity and pressure, which are calculated via the analytical solutions for validation purposes. Two models I and II, both employing the same conditions of Table I but with two different geometries (and necessary meshes) described in Table II, were considered.

Table I
Wave and Fluid (Water) Properties Used for Numerical Modelling

Frequency (Hz)	Amplitude (μm)	Dynamic Viscosity (Pa.s)	Density (kg/m³)
10	1	0.001	1000

Table II
Characteristics of the Computational Domain Used for CFD Calculations

Model	Separation (mm)	Reynold number	Mesh Sizes
I	0.1	62.83	3600 x 60
			1600 x 80
			2000 x 100
II	1	0.793	1500 x 150
			1750 x 175
			2000 x 200

These two models correspond to two Reynolds numbers that differ in magnitude by a factor of approximately 79 (Table II), are used to verify that the solutions developed here are good approximations to the full Navier-Stokes equations. The computational domains are $50\,mm$ and $30\,mm$ for model I and II respectively. The numerical approach method is first described and then followed by a comparison to the analytical solution for different models with a focus on the horizontal and vertical components of the velocity field and pressure drop along the fracture. The approach assumes that the flow is laminar

and incompressible. Therefore, the flow due to compressibility is very small compared to the overall flow created by the squeezing of the parallel walls. This assumption is not valid for highly compressible fluids. In a 2D rectangular geometry, the unsteady Navier-Stokes equations are solved in the finite-volume solver of ANSYS FLUENT *16.2*. The model is made long enough along the $\hat{x}$ direction to minimize edge effects. The geometry consists of two parallel walls; the bottom wall is fixed and the upper is moving to generate an oscillatory displacement causing the contraction and expansion of the distance (thickness) separating the two walls (Fig. 1). The velocity of the upper wall is prescribed as a sinusoidal function of time with amplitude ε and an angular frequency ω implemented in the dynamic mesh tool of the software as a User Defined Function (UDF), which can be written as,

$$\dot{u}_z = -\varepsilon_a \omega \sin\left(\omega t + \frac{\pi}{2}\right) \tag{31}$$

The phase $\frac{\pi}{2}$ is chosen to have an initial velocity, at $t = 0$, set to maximum negative amplitude when the separation of the walls is h_0 while the upper wall is moving downwards. The minus sign is chosen such that the displacement function of the upper wall is given as

$$u_z(t) = \varepsilon_a cos(\omega t + \frac{\pi}{2}) \tag{32}$$

A pressure outlet boundary condition was imposed at the two lateral ends of the fracture to allow the fluid to leave and enter the computational domain as a response to the oscillating upper wall. Explicitly, an atmospheric boundary condition was prescribed at the two pressure outlet boundaries. Different structured rectangular grids were tested to generate a grid-independent solution. For the two considered models the corresponding grids are summarized in Table II. It is worth mentioning that the CFD results considered in the comparison to the analytical solutions represent a smaller region of the computational domains that are $45\ mm$ and $25\ mm$ for model I and II, respectively. The remaining regions containing the pressure boundaries are stripped off to minimize border numerical artefacts. The unsteady simulations were run with an integration time step of $0.5\ ms$ and a second-order implicit scheme was used for time advancement. The convective terms in the solved equations were discretized using a second-order upwind scheme (sometimes advection scheme) which typically refers to a class of numerical discretization methods for solving hyperbolic partial differential equations(35).

III.1 Comparison with Model I

Consider model I with the fluid properties of Table I and the geometry of Table II. In this case the Reynolds number is 62.8, which corresponds to a Stokes number of 7.9. The fluid velocity for the case when only the upper wall (a) is moving upwards and is at a separation of exactly $1\ mm$ and at time $t = 0.05\ s$ (half period) is shown in Fig. 2. The analytical and CFD solutions are shown in Figs. 2(a) and (b) respectively. The analytical and numerical solutions for the velocity field are in excellent agreement with a discrepancy of 0.14%. At this instant, the fluid enters the fracture with a velocity of $1.84\ mm/s$ through both outlets. A good agreement is found for the vertical fluid velocity that reaches a peak of $63.8\ \mu m/s$ near the moving wall with a discrepancy of 0.02%. The same observation can be made for the pressure at $x = 0$ and is $-0.25\ Pa$ with a discrepancy of 0.05% between the two solutions. The horizontal fluid velocity when only the upper wall (a) is moving downwards and is at a separation of exactly $1.000988\ mm$ and at time $t = 0.0775\ s$ is shown in Fig. 3. The analytical and CFD solutions are shown in Figs. 3(a) and (b) respectively. The fluid exits the fracture with a maximum velocity of $0.44\ mm/s$ through both outlets with a discrepancy of 2.18%. The vertical fluid velocity reaches a negative peak of $-9.83\ \mu m/s$ near the moving wall with a discrepancy of 3.11%. The pressure at $x = 0$ is $1.18\ Pa$ with a discrepancy of 0.02%. It is readily noticeable that the fluid starts to flow horizontally near the walls while it has not yet reversed course at the middle of the gap. All solutions in this case are also in good agreement. Analytical and CFD pressure distribution and horizontal fluid velocity profiles at the position pointed at by the black arrow in a) and b). The maximum fluid velocity and pressure are 1.84 mm/s and 0.25 Pa, respectively.

The fluid velocity when only the upper wall (a) is moving downwards and is at a separation of exactly $1.000707\ mm$, corresponding to time $t = 0.0875\ s$, is shown in Fig. 4. The analytical and CFD solutions are shown in Figs. 4(a) and (b) respectively. The fluid exits the fracture with a maximum velocity of $1.18\ mm/s$ through both outlets. The two solutions are in good agreement with a discrepancy of 0.54%. The vertical fluid velocity reaches a negative peak of $-44.43\ \mu m/s$ near the moving wall with a discrepancy of 0.41%. The pressure at $x = 0$ is $1.00\ Pa$ with a discrepancy of 0.03%. Again, all solutions are in good agreement. It is important to point out that there is a vertical exaggeration of *~14.8* for all displayed results in Figs. 2, 3, and 4. It is also important to mention that the fluid velocity is dominated largely by the horizontal fluid velocity.

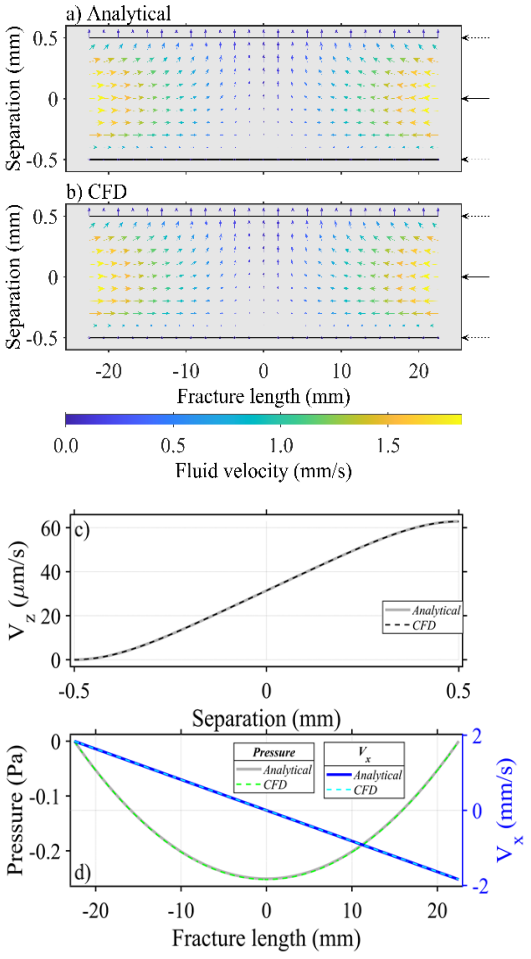

Figure 2. a) and b): Fluid velocity simulations using model I (Tables 1 and 2) at time t=0.0500 s (half period) when the fracture upper wall (a) is moving upwards, and bottom wall (b) is fixed, and the separation between the walls is 1 mm a) shows the analytical and b) the CFD results. There is a vertical exaggeration of ~14.8. c) Analytical and CFD vertical fluid velocity. d)

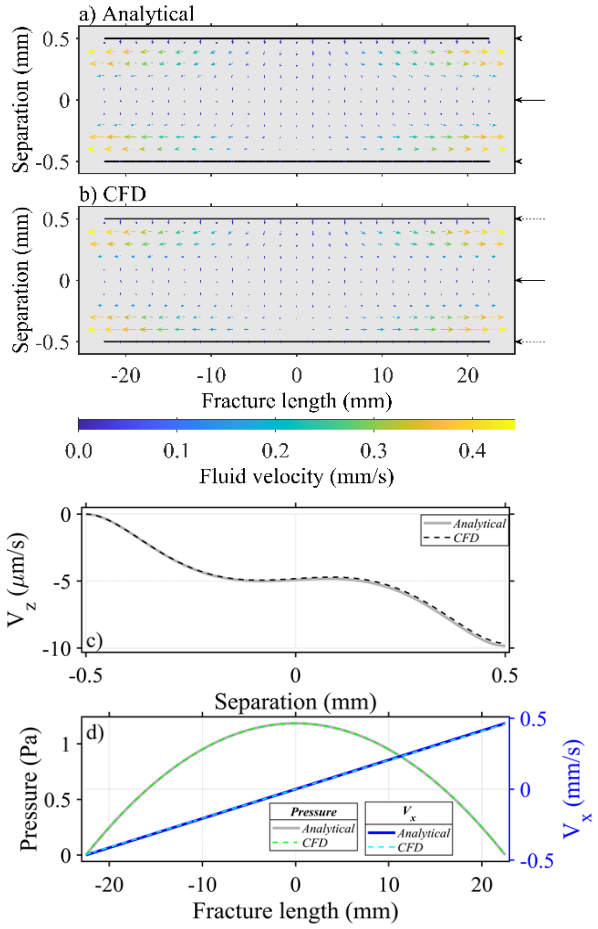

Figure 3. a) and b): Fluid velocity simulations using model I (Tables 1 and 2) at time t=0.077500s s (half period) when the fracture upper wall (a) is moving upwards, and bottom wall (b) is fixed, and the separation between the walls at rest is 1.000988 mm a) shows the analytical and b) the CFD results. There is a vertical exaggeration of ~14.5:1. c) Analytical and CFD vertical fluid velocity. d) Analytical and CFD pressure distribution and horizontal fluid velocity profiles at the position pointed at by the black arrow. The maximum fluid velocity and pressure are 0.47 mm/s and 1.18 Pa, respectively.

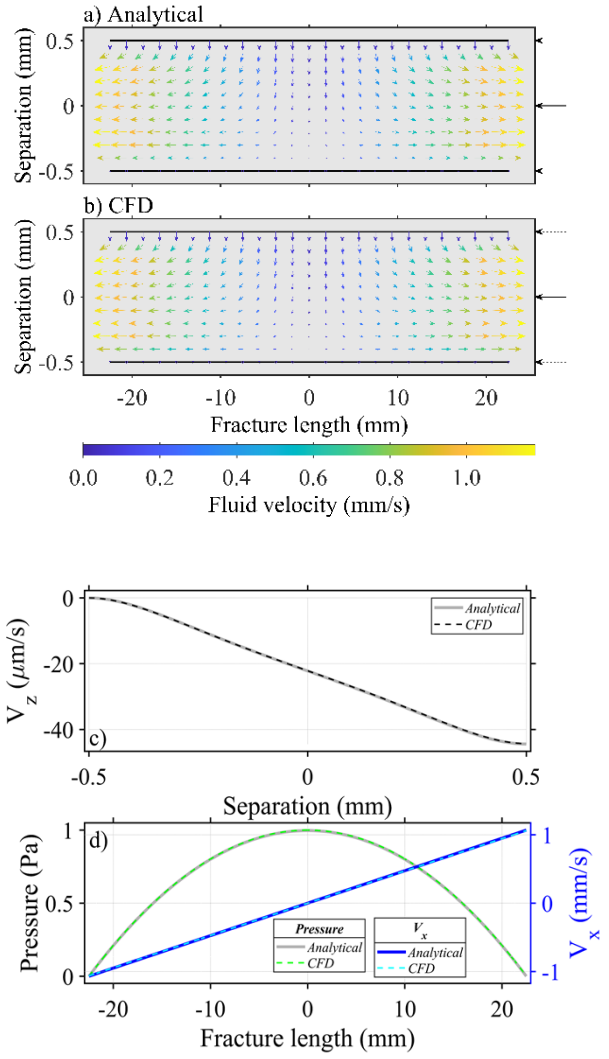

Figure 4. a) and b): Fluid velocity simulations using model I (Tables I and II) at time $t = 0.087500$ s when the upper wall (a) is moving downwards, and bottom wall (b) is fixed, and the separation between the two fracture walls at rest is 1.000707 mm a) shows the analytical and b) the CFD results. There is a vertical exaggeration of ~14.5:1. The small circles show a nil velocity field. c) Analytical and CFD vertical fluid velocity. d) Analytical and CFD pressure distribution and horizontal fluid velocity profiles at the position pointed at by the black arrow. The maximum fluid velocity and pressure are 1.20 mm/s and 1.00 Pa, respectively.

III.2 Comparison with Model II

Consider model II with the geometry and fluid properties are given in Tables I and II. In this case the Reynolds number is 0.6 which corresponds to a Stokes number of 0.8. The horizontal fluid velocity when only the upper wall (a) is moving upwards and is at a separation of exactly $0.1\ mm$ and at time $t = 0.05\ s$ (half period) is shown in Fig. 5. The analytical and CFD solutions are shown in Figs. 5(a) and (b) respectively. The fluid enters the fracture with a maximum velocity of $11.73\ mm/s$ through both outlets. The results are in good agreement with a discrepancy of 0.27%. The vertical fluid velocity reaches a peak of $-62.8\ \mu m/s$ near the moving wall with a discrepancy of *0.13%*. The pressure-drop at $x = 0$ is $-58.9\ Pa$ is relatively to

the extremities of the fracture. These are also in good agreement with 0.25% discrepancy.

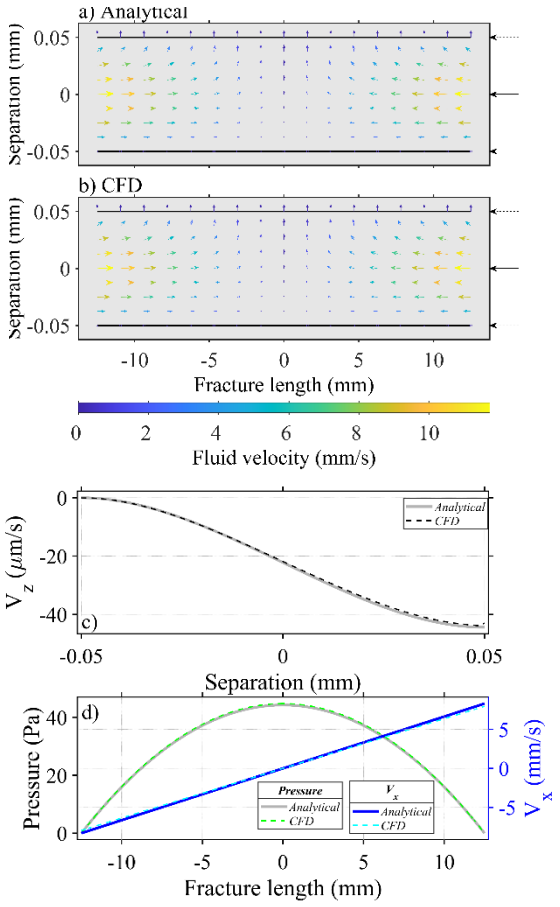

Figure 5. a) and b): Fluid velocity simulations using model II (Tables I and II) at time $t = 0.0500\ s$ when the upper wall (a) is moving upwards, and bottom wall (b) is fixed, and the separation between the two fracture walls is $0.1\ mm$ a) shows the analytical and b) the CFD results. There is a vertical exaggeration of ~76.4. c) Analytical and CFD vertical fluid velocity. d) Analytical and CFD pressure distribution and fluid velocity profiles at the position pointed at by the black arrow. The maximum fluid velocity and pressure are 11.73 mm/s and -58.91 Pa respectively.

The fluid velocity when only the upper wall (a) is moving downwards and is at a separation of exactly $0.100707\ mm$ and at time $t = 0.0875\ s$ is shown in Fig. 6. The analytical and CFD solutions are shown in Figs. 6(a) and (b) respectively. The fluid exits the fracture with a maximum velocity of $8.27\ mm/s$ through both outlets. The two solutions are in good agreement with a discrepancy of 4.27%. The vertical fluid velocity reaches a negative peak of -44.43 μm/s near the moving wall with a discrepancy of 2.42%. The pressure at x=0 is 44.27 Pa with a discrepancy of 0.11%. It is also important to point out that, in this case, there is a vertical exaggeration of ~75.8 for all displayed results in Figs. 5-6 (a) and (b). The fluid velocity is dominated largely by the horizontal fluid velocity. Considering the results presented here, the small oscillations approximation led to analytical solutions based on similarity arguments, which agree with the numerical solutions obtained with the full set of the Navier-Stokes equations in a two-dimensional situation giving more confidence in the validity of our results within small

acoustic oscillations. The analytical solutions are advantageous because they are extremely fast to compute compared to the numerical solutions. Furthermore, these solutions can be used directly in other applications where analytical solutions and speed are essential. However, these solutions are for incompressible fluids, and further developments are needed to extend the analysis to non-Newtonian fluids as well as quantifying transmissivity and reflectivity of seismic waves at planar saturated fractures where fluid-compressibility must be accounted for.

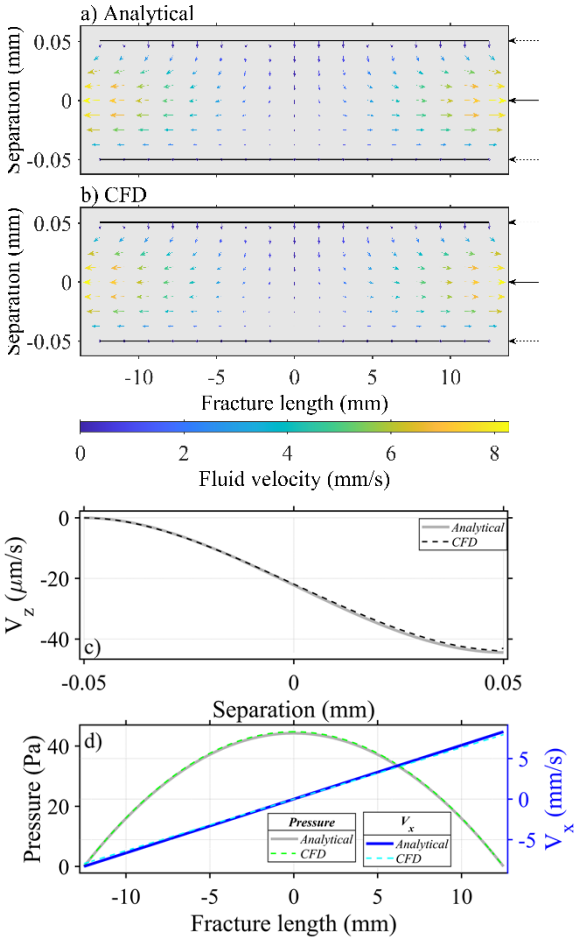

Figure 6. a) and b): Fluid velocity simulations using model II (Tables I and II) at time $t = 0.0875\ s$ when the upper wall (a) is moving downwards, and bottom wall (b) is fixed, and the separation between the plates is $0.100707\ mm$. a) shows the analytical and b) the CFD results. There is a vertical exaggeration of ~75.8. c) Analytical and CFD vertical fluid velocity. d) Analytical and CFD pressure distribution and horizontal fluid velocity profiles at the position pointed at by the black arrow. The maximum fluid velocity and pressure are 8.27 mm/s and 44.27 Pa, respectively. The maximum fluid velocity and pressure are 8.27 mm/s and 44.27 Pa, respectively.

IV. Modeling Experiments: Effect of Facture and Wave Properties

IV.1 Impact of fracture length and opening on fluid-flow

For modeling simulations, consider a fracture with two parallel walls with a gap filled with a fluid (water, viscosity of 1 mPa.s.) (Fig. 1). Let the vibration be a harmonic oscillation with a frequency of 20 Hz and an amplitude of 1 μm. The real and imaginary

parts of the function f(ξ) and its first derivative are shown in Figs. 7(a) and (b) when the walls vibrate out of phase by $180°$. The solutions exhibit symmetries as illustrated in Figs. 7(a) and (b) for models with a varying gap between 0.1 mm and 2 mm corresponding to Stokes number between 1.1 and 22.4. Both the real and imaginary parts of f(ξ) are symmetrical, about the origin for all models. However, both the real and imaginary parts of f'(ξ) are symmetrical about ξ=0. It is worth mentioning that the Stokes number s increases with increasing frequency as well as with an increasing gap between the fracture walls. Fig. 7c) and d) show the maximum pressure change along the fracture for various fracture lengths as a function of fracture aperture (Fig. 7c). The pressure change, for various fracture apertures, as a function of fracture length is shown in Fig. 7d. Evidently the pressure variation increases with increasing fracture length as well as with decreasing fracture opening. Since the horizontal velocity of the fluid flow is dependent on the first derivative of f (f^') we also investigate the variation of this velocity with varying Stokes number. The real and imaginary parts of the first derivative f^' and the horizontal fluid velocity are displayed in Figs.8 a-b and 8 d-e with varying Stokes number. Again here, the frequency of the oscillation is 20 Hz, and the Stokes number varies with the varying separation of the walls of the fracture model. The horizontal velocity vertical profile is given at the extremity of the fracture (Figs. 8 c) and 8 f). We can see that for small Stokes numbers the front of the fluid flow is parabolic (Fig. 8c) whereas it becomes nearly flat for large Stokes numbers (Fig. 8f). The horizontal fluid velocity is highly dependent on the function $f'(\xi)$ which is modulated by the velocity difference of the fracture walls.

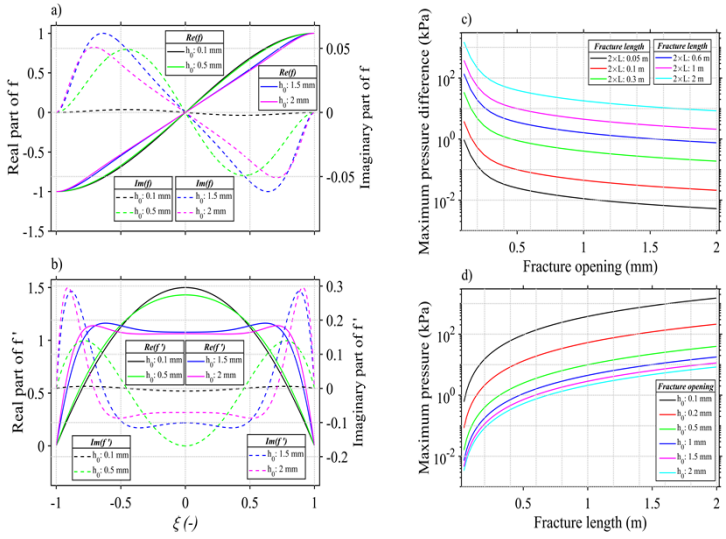

Figure 7. a) and b) show the real and imaginary parts, of f and f' respectively, for various fracture openings h_0 between 0.1 mm and 2 mm corresponding to a range of Stokes number of 1.1-22.4. The frequency of the oscillations is 20 Hz and the fluid is water. The amplitude of the oscillation is 1 μm. c) Maximum pressure-drop for various fracture lengths (see legend) as a function of fracture opening. d) Pressure-drop for various fracture openings (see legend) as a function of fracture length. The frequency of the oscillations is 20 Hz and the fluid is water.

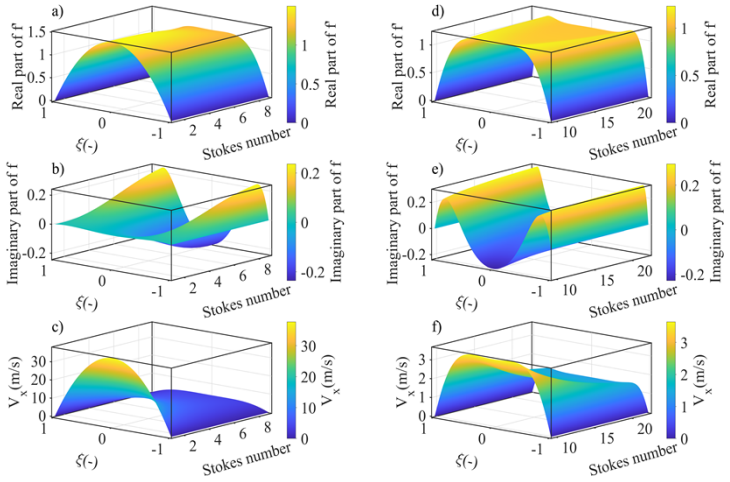

Figure 8. a) and b) are the real and imaginary parts of f' respectively for small Stokes numbers. c) is the horizontal fluid velocity at small Stokes numbers. d) and e) are the real and imaginary parts of f' respectively for relatively larger Stokes numbers than those of a) and b). f) is the corresponding horizontal fluid velocity. The frequency and amplitude of the wave are 20 Hz and 1μm respectively.

IV.2 Waves on fluid-flow in the presence of a pressure gradient

In this section we investigate the fluid flow when a pressure gradient is present between the inlet and outlet of a fracture with parallel walls under typical reservoir pressure. The pressure at the fracture inlet (left side of Fig. 1) is higher than that of the outlet (right side of Fig. 1) with a pressure gradient of 0.45 psi/ft with a reservoir average pressure of 2000 psi. In the absence of vibrations, the velocity and pressure are shown in Figs. 9a) and b) for water. We will consider three fracture models saturated with water, oil, and toluene. The wave and fracture properties are given in Table III whereas the reservoir and fluid properties are given in Table IV. For the case where the fracture is saturated with water, the simulations are shown in Figs. 10 and 11. When vibration occurs, the velocity varies with time as shown in Fig. 10. We notice that there is no more symmetry, a consequence of the presence of the pressure gradient. It is also found that fluid accelerates back and forth with a high acceleration (Fig. 11). This suggests that when solvents are injected in an oil reservoir along seismic vibration near the well-bore, the induced shaking of the fluid can improve the dissolution of oil in solvents and consequently, can increase oil production. The vibration not only creates a vertical flow but also creates a more significant flow laterally with high acceleration and deceleration along the fracture length.

Table III
WAVE AND FRACTURE PROPERTIES USED FOR NUMERICAL EXPERIMENTS

Frequency (Hz)	**Wave Amplitude walls (a) and (b) (μm)**	**Fracture length (cm)**	**Fracture gap (mm)**
20	20 and 10	20	0.8

Table IV
RESERVOIR AND FLUID PROPERTIES USED FOR NUMERICAL EXPERIMENTS

Fluid	Reservoir pressure (psi)	Pressure gradient (psi/ft)	Viscosity (cP)	Density (kg/m^3)
Water	2000	-0.45	1.0	1000
Crude oil			6.6	953
Toluene			0.560	853

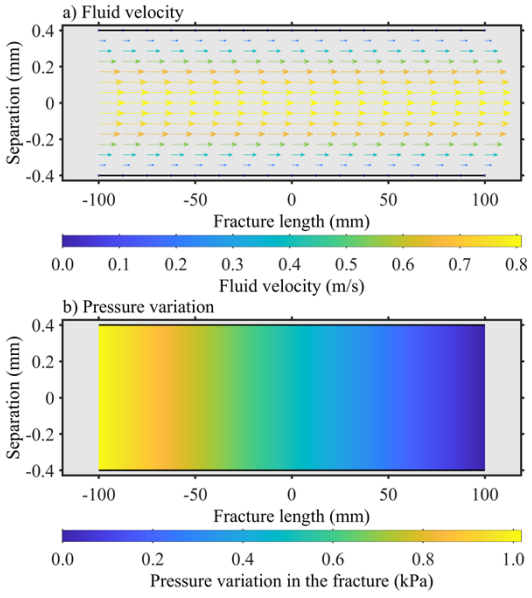

Figure 9. a) Velocity field created by the pressure gradient in the fracture. b) Pressure variation along with the fracture. The frequency of oscillations is 20 Hz and the fluid is water. The vertical exaggeration is 93.7.

The fluid velocity and acceleration at the right outlet of the fracture variation with time is shown in Fig. 12 a) and b) respectively during one time-period of the oscillation (.05 s). We notice fluid pressure variations along the fracture midway between the fracture walls within one time-period of the oscillation (Fig. 12c). This is a significant pressure change compared to the lone pressure gradient result shown in Fig. 9a. The pressure variation due to the vibration alone (see Figs. 2-6) exhibits a symmetry about the center of the fracture. This shows that there is no increase or decrease of flow at the outlet of the fracture during a time-period. Indeed, calculating the fluid volume exiting the fracture for the lone presence of the pressure gradient and that with the presence of both vibration and pressure gradient it is found that these are identical and is ~434.02 cm3/s for a fracture with an aperture of 0.8 mm and a length of 20 cm. The conservation of mass is verified by calculating the volume entering and exiting the fracture within a time-period which is found to be the same.

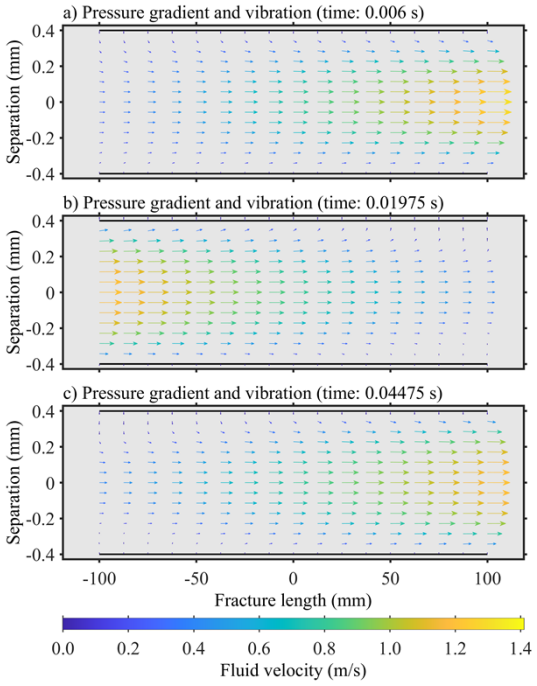

Figure 10. Three snapshots of water velocity simulations along the fracture during one time-period (0.05s). The vertical exaggeration is 91.7.

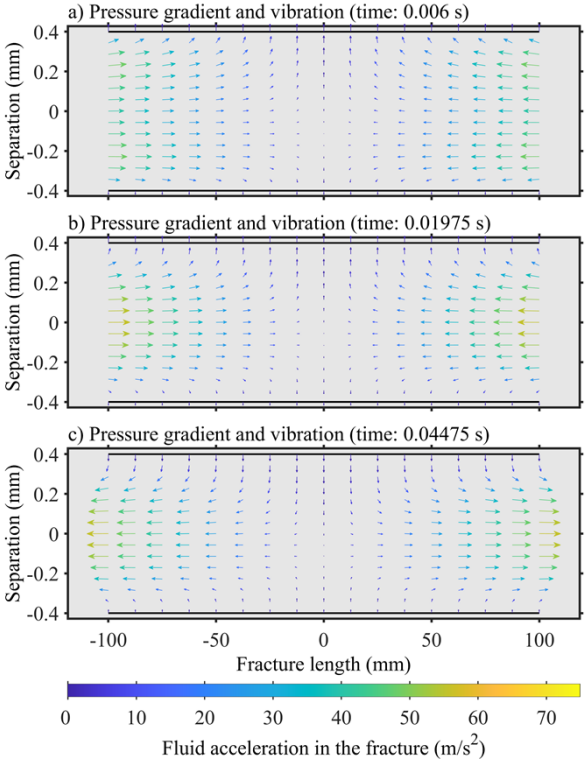

Figure 11. Three snapshots (same times as Fig.10 of water acceleration simulations along the fracture during one time-period (0.05s). The vertical exaggeration is 91.7.

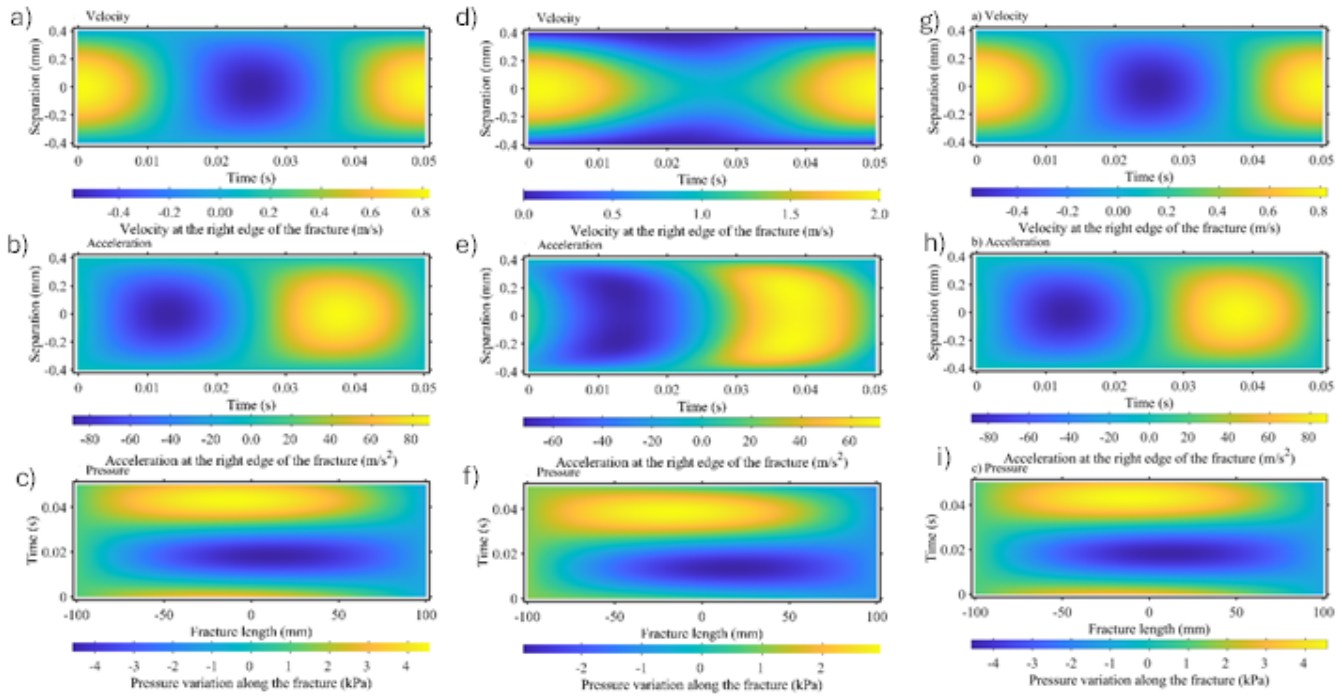

Figure 12. a), d) Velocity simulations at the right outlet of the fracture during one time-period (0.05s) using the model of Tables III and IV for water and oil. b), e) Fluid acceleration. c), f) Pressure variation along the fracture length. The left, middle and right columns display simulation results of water, crude oil and toluene, respectively.

In the case where the fracture is saturated with oil, we obtain the same relative results (Fig. 13). However, the fluid velocity and pressure variations, are relatively smaller than those when the fluid is water. The crude oil output at the outlet and input at the inlet in one period is 65.76 cm3/s. The volume in this case is much smaller than that of the case of water. Obviously, the viscosity plays a major role in the velocity field. In the case of a toluene–saturated fracture, we also obtain the same relative results (Fig. 14). However, the fluid velocity and pressure variations, are relatively higher and more significant than those when the fluid is water. The fluid output at the outlet and input at the inlet in one period is 775.04 cm^3/s. The volume in this case is much larger than that of the case of water. Obviously, the viscosity plays a major role in the velocity field and acceleration. The fluid velocity and acceleration decrease with increasing viscosity in the case of the presence of the pressure gradient alone (Solid lines in Fig. 15). These tend to converge to a small value at higher viscosity. However, the induced velocity by the seismic vibrations (Dashed lines Fig. 15) tend to a constant that increases with decreasing fracture wall separation. These results can influence oil production and will be discussed below.

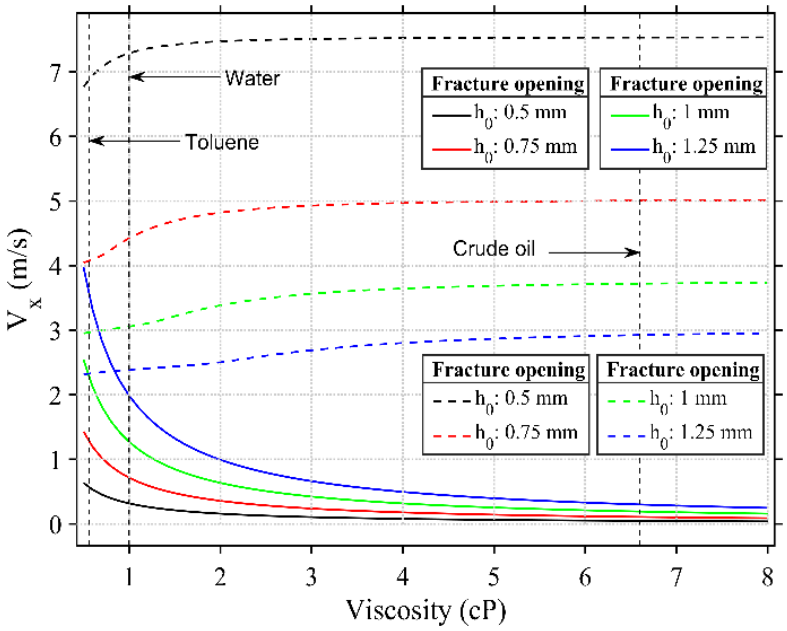

Figure 13. Maximum horizontal velocity for various fracture openings ($\boldsymbol{h_0}$) versus fluid viscosity. The solid lines are velocities for the lone pressure gradient and the dashed lines are the induced velocities by the lone seismic vibration. The vertical dotted line highlights the velocities for various fracture openings when the saturating fluid is water, toluene, and crude oil.

V. DISCUSSION

The proposed fluid-saturated fracture model, with horizontal and parallel walls, is based on a narrow gap assumptions and small oscillations. The approach used here led to a new closed form for the fluid pressure distribution and can be regarded as a model between lubrication, where the viscous flow dominates inertial terms, to the full Navier-Stokes equations as proposed by Ishizawa (36). Therefore, the flow is assumed to be laminar.

Besides the academic interest of the approach, the developed analytical solutions can be useful in practical applications ranging from ultrasonic probing for cracks in materials through to seismic characterizations of geological formation where fluids play an important role, such as oil reservoirs. As mentioned earlier, the goal of this contribution is to apply this model to oil reservoirs through the study of the behavior of fluids as seismic waves impinge onto both natural and induced fractures in oil reservoirs. This can be particularly of interest in enhanced oil recovery where the technique can be used to stimulate oil flow to a producing well of a fractured reservoir. It has been found that the induced fluid pressure in cracks and fractures depends on the separation between the walls of the fracture, the type of fluid in the fracture, and the amplitude and frequency of the seismic oscillations. The induced horizontal flow is cyclical and oscillates according to the seismic wave frequency. This oscillatory flow is embedded on the top of the background flow and can be more prominent under certain conditions. Enhanced

oil recovery can be achieved by injection under high pressure of various fluids such as solvents. Seismic waves can create a local flow in horizontal fractures that oscillates along the fracture length. This shaking of the fluid is shown to not hinder the flow due to pressure gradient. Therefore, it does not increase production by flow but instead by helping to improve the mixing of the fluids in the fracture such as solvents and crude oil. This will lead to an improved oil recovery. However, this can only be efficient under certain conditions. A parameter to consider is the amplitude of the wave. Assuming a small ratio of 0.05 between the two Reynolds numbers R_1 and R_2 as described above, the amplitude of the wave should not exceed $0.05 \times h_0$, in other words the amplitude of the wave should not exceed 5% of the gap between the fracture walls. Typically, fractures are of submillimeter in thickness and seismic amplitudes impinging onto oil reservoirs have amplitudes that are, generally, of few micrometers in displacement which correspond to the models presented in this contribution.

Fractures play a very important role in oil reservoirs as they directly impact production. A good characterization of an oil reservoir to extract fracture networks information such as density, orientation, fluid content, thickness, and length of fractures are crucial for reservoir development and production optimization. It is well known that fractures scatter seismic energy at the top and bottom walls of a fracture as reflected P and transmitted P, respectively at normal incidence. These make the walls vibrate, generally, with different amplitudes which are dependent of the properties of materials involved. Therefore, the proposed fracture model can be used for seismic waves as the developed solutions do not impose equal amplitudes nor the 180^o phase difference of vibrating walls in contrast with the model proposed by Thorpe (28) and others. Moreover, at seismic amplitudes, which are generally very small at the reservoir level, we can neglect all second order terms in the Navier-Stokes equations as proposed here which allows to employ the principle of superposition, a concept accepted and used in seismic data processing.

We have shown that the fluid flow velocity field has two components (see (22)) and is highlighted by the numerical simulations. On one hand, a vertical component is induced by the vibration that is maximum at the wall and decays away from it. On another hand, a horizontal component that is nil at the center and increases away from the center in both lateral directions (see (23)). Its absolute maximum is reached at the left and right borders of the fracture with opposite signs. The horizontal component is quite significant and dominates the overall flow. Therefore, the fluid is shaking in both the vertical and horizontal directions but prominently in the horizontal direction. It is also found that the induced fluid flow does not alter the background fluid flow induced by the presence of a pressure gradient. We have also seen through the numerical experiments given above that the type of fluid influences the overall flow.

To optimize production, a testing of parameters should be considered through a feasibility study. At an onshore site for example, an array of vibrators above the reservoir can be operated simultaneously to create a pseudo-plane wave (i.e., a large beam) with varying the controlling factors that are amplitudes and frequencies to find optimal values through real-time monitoring of production. A good characterization of the fractures at the reservoir level could be conducted to extract information on the fractures to aim at the correct range of amplitudes of the seismic waves, the radial extent of the reservoir, and fracture orientation.

VI. CONCLUSIONS

In the frame of seismic oscillations, an approximation to the Navier-Stokes equations for a steady squeeze flow between two parallel walls of a fluid-saturated fracture is solved analytically to obtain the fluid pressure variation along the fracture as well as the fluid velocity by assuming that the fluid is incompressible. The analytical solutions for the horizontal and vertical fluid flow velocities and the pressure variation along the fracture were developed without restrictions on the relative phases and amplitudes of a fracture's vibrating walls through the principle of superposition. This is particularly true for seismic waves traveling through interfaces between geological formations and fractures where waves are reflected and transmitted with differing amplitudes and phases in general. These analytical solutions were compared with the numerical solutions obtained via a computational fluid dynamics scheme based on finite volume using the full form of the Navier-Stokes equations containing the non-linear inertia terms. These are found to be in good agreement with each other which gives more confidence to the accuracy of the proposed approximation. The solutions indicate that the pure squeezing motion governs the pressure generated by the force acting on the walls. This can be regarded as a possible mechanism that can stimulate oil recovery. It is found that the squeezing motion induces an oscillatory flow along the fracture length, between the horizontal fracture walls and can be very large for certain sets of parameters and reservoir conditions. The amplitude of the oscillatory flow increases with frequency, fracture length, and decreasing separation of the walls. This mechanism can mobilize fluids and stimulate the mixing of injected fluids with crude oil in a reservoir. Therefore, it can explain the improved oil recovery reported in some literature through seismic stimulation near a producing well. The stimulation can be achieved through an array of synchronized vibrators above a fractured reservoir to create a pseudo-plane wave (large beam). Conducting tests by varying amplitude and frequency of the vibrations and characterizing the fractures can help in optimizing these parameters to achieve an improved oil recovery at an oil producing well. This process can work better for near-horizontal fractures where the gap is small with respect to the length of the fracture. The longer the fracture is, the more prominent the induced oscillatory flow within the fracture. This induced flow will not increase the background flow average but rather improve the mixing of fluids within the

fracture, particularly during an enhanced oil recovery process through injection of solvents. The vibration creates a high acceleration that can detach oil and increase the mixture's crude oil/solvent ratio

ACKNOWLEDGMENT

The authors are grateful to Khalifa University of Science and Technology (KUST) for providing the High-Performance Computing facility for the CFD calculations and for supporting this work.

REFERENCES

1. Beresnev IA, Johnson PA. Elastic-wave stimulation of oil production; a review of methods and results. Geophysics. 1994;59(6):1000-17.
2. Irfan M, Lenn CP, Ghosh D, editors. Seismic Stimulation and Induced Seismicity in Oil Reservoirs: A Review of Applications to Enhanced Oil Recovery (EOR). ICIPEG 2016; 2017 2017//; Singapore: Springer Singapore.
3. Sun Q, Retnanto A, Amani M. Seismic vibration for improved oil recovery: A comprehensive review of literature. International Journal of Hydrogen Energy. 2020;45:14756-78.
4. Wooden B. Technology Update: Seismic Stimulation: An Eco-Friendly, Effective EOR Alternative. Journal of Petroleum Technology. 2018;70(08):21-3.
5. Pride S, Flekkøy E, Aursjø O. Seismic stimulation for enhanced oil recovery. Geophysics. 2008;73.
6. Allahverdiyev PQ. Improved sweep efficiency through seismic wave stimulation. Austin Texas: The University of Texas at Austin,; 2012.
7. Kouznetsov OL, Simkin EM, Chilingar GV, Katz SA. Improved oil recovery by application of vibro-energy to waterflooded sandstones. Journal of Petroleum Science and Engineering. 1998;19(3):191-200.
8. Westermark RV, Brett JF, Maloney DR. Enhanced Oil Recovery with Downhole Vibration Stimulation. SPE Production and Operations Symposium2001. p. SPE-67303-MS.
9. Gutierrez M, Youn D-J. Effects of fracture distribution and length scale on the equivalent continuum elastic compliance of fractured rock masses. Journal of Rock Mechanics and Geotechnical Engineering. 2015;7(6):626-37.
10. Bouchaala F, Ali MY, Matsushima J, Bouzidi Y, Takam Takougang EM, Mohamed AA, et al. Azimuthal investigation of compressional seismic-wave attenuation in a fractured reservoir. Geophysics. 2019;84(6):B437-B46.
11. Takougang EMT, Ali MY, Bouzidi Y, Bouchaala F, Sultan AA, Mohamed AI. Characterization of a carbonate reservoir using elastic full-waveform inversion of vertical seismic profile data. Geophysical Prospecting. 2020;68(6):1944-57.
12. Futterman WI. Dispersive body waves. Journal of Geophysical research. 1962;67(13):5279-91.
13. Pyrak-Nolte LJ, Myer LR, Cook NG. Transmission of seismic waves across single natural fractures. Journal of Geophysical Research: Solid Earth. 1990;95(B6):8617-38.
14. Rozhko AY. On spectral changes of seismic wave energy by a partially saturated crack due to the hysteresis of liquid bridges phenomenon. Geophysics. 2021;86(3):MR133–MR47.
15. Pecheux B, Bonneau O, Frêne J. Investigation about Electrorheological Squeeze Film Damper Applied to Active Control of Rotor Dynamic. International Journal of Rotating Machinery. 1997;3(1).
16. Mabuchi K, Sasada T. Numerical analysis of elastohydrodynamic squeeze film lubrication of total hip prostheses. Wear. 1990;140(1):1-16.
17. Cookson RA, Kossa SS. The effectiveness of squeeze-film damper bearings supporting rigid rotors without a centralising spring. International Journal of Mechanical Sciences. 1979;21(11):639-50.
18. Kumar HNA, Shilpashree DJ, Adarsh MS, Amith D, Kulkarni S. Development of Smart Squeeze Film Dampers for Small Rotors. Procedia Engineering. 2016;144:790-800.
19. Jin ZM, Dowson D, Fisher J. Analysis of fluid film lubrication in artificial hip joint replacements with surfaces of high elastic modulus. Proceedings of the Institution of Mechanical Engineers, Part H: Journal of Engineering in Medicine. 1997;211(3):247-56.
20. Unsworth A, Dowson D, Wright V. Some new evidence on human joint lubrication. Annals of the Rheumatic Diseases. 1975;34(4):277-85.
21. Guo Z, Hirano T, Kirk RG. Application of CFD Analysis for Rotating Machinery: Part 1 — Hydrodynamic, Hydrostatic Bearings and Squeeze Film Damper. 2003(36878):651-9.
22. Tichy JA, Winer WO. Inertial Considerations in Parallel Circular Squeeze Film Bearings. Journal of Lubrication Technology. 1970;92(4):588-92.
23. Pandey A, Pratap R, Siong Chau F. Influence of Boundary Conditions on the Dynamic Characteristics of Squeeze Films in MEMS Devices2007. 893-903 p.
24. Pandey AK, Pratap R. A comparative study of analytical squeeze film damping models in rigid rectangular perforated MEMS structures with experimental results. Microfluidics and Nanofluidics. 2007;4: 205-18.
25. Feixia P, Joel K, Eric P, Alex TT, Subrata M. Squeeze film damping effect on the dynamic response of a MEMS torsion mirror. Journal of Micromechanics and Microengineering. 1998;8(3):200.
26. Murakami T, Higaki H, Sawae Y, Ohtsuki N, Moriyama S, Nakanishi Y. Adaptive multimode lubrication in natural synovial joints and artificial joints. Proceedings of the Institution of Mechanical Engineers, Part H: Journal of Engineering in Medicine. 1998;212(1):23-35.
27. Livesey JL. Inertia effects in viscous flows. International Journal of Mechanical Sciences. 1960;1(1):84-8.
28. Thorpe JF. Further Investigation of Squeezing Flow between Parallel Plates. Developments in theoritical and applied mechanics. 1967;3:635-48.
29. Gupta PS, Gupta AS. Squeezing Flow between Parallel Plates. Wear, Elsevier. 1977;45:177-85.
30. Minhang B, Heng Y. Squeeze film air damping in MEMS. In Sensors and Actuators A: physical. 2007;136(1):3-27.
31. Jackson JD. Applied Scientific Research. 1962;Sec. A, 11(1):148-52.
32. Gomberg J, Johnson P. Dynamic triggering of earthquakes. . Nature; 2005. p. 830.
33. D.P. H, S.G. P. Dynamic Triggering. Treatise on Geophysics ed: Elsevier; 2007.
34. Wikes JO. Fluid Mechanics for Chemical Engineers: with Microfluidics, CFD, and COMSOL Multiphysics 5: Pearson; 2017. 816 pages p.

35. Ansys. Fluent User's Guide. Canonsburg, PA: Ansys, Inc.; 2010. p. 653.
36. Ishizawa S. The Unsteady Laminar Flow between Two Parallel Discs with Arbitrary Variying Gap Width. Bulletin of JSME. 1966;9(35):533-50.